World Conference on
Timber Engineering
Oslo 2023

SEISMIC PERFORMANCE EVALUATION OF REINFORCED WOODEN TEMPLE BASED ON LONG TERM EARTHQUAKE OBSERVATIONS

Toshiaki Sato[1], Yasuhiro Nambu[2], Yuji Miyazu[3] and Masayuki Nagano[4]

ABSTRACT: The seismic performance of structures is known to change over time, and the causes are affected by the surrounding environment such as temperature and humidity as well as damage caused by disturbances such as earthquakes. In terms of structure, seismic performance has been evaluated based on the construction age, mainly the transition of related laws and regulations, but the seismic performance changes over time, considering the material properties that swell and shrink sensitively due to temperature and humidity. the purpose of this study is to quantitatively evaluate the effects of various influential factors using earthquake observation records which are measured over a long period of time at the main hall of wooden temple. The subspace method was applied to the observation record of target temple, and the transition of the natural frequency due to aging was verified as the environment was changed. As a result of the investigation, the natural frequency changed as the temperature up and down, suggesting the effect of swell and shrink of the joint. Further, in the deformation range about less 3 mm, the variation in the natural frequency may have the same effect as the nonlinearity due to the large and small response.

KEYWORDS: System Identification, Subspace Method, Traditional Wooden buildings

1 INTRODUCTION

The seismic performance of structures is known to change over time, and the causes are affected by the surrounding environment such as temperature and humidity as well as damage caused by disturbances such as earthquakes. In terms of structure, seismic performance has been evaluated based on the construction age, mainly the transition of related laws and regulations, but the seismic performance changes over time, considering the material properties that swell and shrink sensitively due to temperature and humidity in case of timber structure. On the other hand, there is still no way to quantitatively evaluate the seismic performance of the wood structure over time, and it can be said that the accumulation of knowledge is indispensable.

Against this background, the purpose of this study is to quantitatively evaluate the effects of various influential factors using earthquake observation records which are measured over a long period of time at the main hall of wooden temple shown in Fig. 1. In this paper, we first organize the system identification method by the subspace methods used in the subsequent studies, and then describe the results of the analysis focusing on the transition of the natural freq-uency together with the identification results by the earthquake observation records.

***Figure 1**: Photo of the target temple*

2 SYSTEM IDENTIFICATION BASED ON SUBSPACE METHOD

2.1 NUMERICAL CALCULATION BY ORDINARY MOESP METHOD

Since the subspace method has the advantage of being applicable to multi-input multi-output (MIMO) systems, verification work of its identification accuracy has been advanced in previous studies, and considering its significance in this study, the Ordinary MOESP method was adopted. In the subspace method, it is considered that

[1] Toshiaki Sato, Dr. Eng., Assoc. Prof., Kyushu University, Japan, sato@arch.kyushu-u.ac.jp
[2] Yasuhiro Nambu, Dr. Eng., Assist. Prof., Kyushu University, Japan, nambu@arch.kyushu-u.ac.jp
[3] Yuji Miyazu, Dr. Eng., Assoc. Prof., Tokyo University of Science, Japan, miyazu@rs.tus.ac.jp
[4] Masayuki Nagano, Dr. Eng., Prof., Tokyo University of Science, Japan, nagano-m@rs.tus.ac.jp

https://doi.org/10.52202/069179-0306

each expression in Eqs. (1) and (2) are satisfied as the state-space representation of the discrete-time linear time-invariant system of m input l output [1].

$$\mathbf{x}(k+1) = \mathbf{A}\,\mathbf{x}(k) + \mathbf{B}\,\mathbf{u}(k) + \mathbf{w}(k) \tag{1}$$

$$\mathbf{y}(k) = \mathbf{C}\,\mathbf{x}(k) + \mathbf{D}\,\mathbf{u}(k) + \mathbf{v}(k) \tag{2}$$

Where, $\mathbf{x}(k)$ denotes the state vector, $\mathbf{u}(k)$ and $\mathbf{y}(k)$ are the input to the system and the output of the system, respectively. **A**, **B**, **C** and **D** are the constant matrix. These vectors and matrices belong to a set of real numbers. $\mathbf{w}(k)$ and $\mathbf{v}(k)$ are unmeasurable vector signals. They are assumed to be zero mean, stationary, white noise vector sequences. The Eqs. (1) and (2) can be organized as

$$\mathbf{Y} = \mathbf{\Theta}\,\mathbf{X} + \mathbf{\Psi}\mathbf{U} + \mathbf{\Xi}\mathbf{W} + \mathbf{V}\,. \tag{3}$$

Where, **U** and **Y** denote the Input and output block Hankel matrices, respectively, and **X** is matrix composed by state vectors. These are expressed as follows.

$$\mathbf{U}_p = \begin{bmatrix} \mathbf{u}(k) & \mathbf{u}(k+1) & \cdots & \mathbf{u}(k+N-1) \\ \mathbf{u}(k+1) & \mathbf{u}(k+2) & \cdots & \mathbf{u}(k+N) \\ \vdots & \vdots & \ddots & \vdots \\ \mathbf{u}(k+r-1) & \mathbf{u}(k+r) & \cdots & \mathbf{u}(k+r+N-2) \end{bmatrix}$$

$$\mathbf{U}_f = \begin{bmatrix} \mathbf{u}(k+r) & \mathbf{u}(k+r+1) & \cdots & \mathbf{u}(k+r+N-1) \\ \mathbf{u}(k+r+1) & \mathbf{u}(k+r+2) & \cdots & \mathbf{u}(k+r+N) \\ \vdots & \vdots & \ddots & \vdots \\ \mathbf{u}(k+2r-1) & \mathbf{u}(k+2r) & \cdots & \mathbf{u}(k+2r+N-2) \end{bmatrix}$$

$$\cdots \text{(4-1, 2)}$$

$$\mathbf{Y}_p = \begin{bmatrix} \mathbf{y}(k) & \mathbf{y}(k+1) & \cdots & \mathbf{y}(k+N-1) \\ \mathbf{y}(k+1) & \mathbf{y}(k+2) & \cdots & \mathbf{y}(k+N) \\ \vdots & \vdots & \ddots & \vdots \\ \mathbf{y}(k+r-1) & \mathbf{y}(k+r) & \cdots & \mathbf{y}(k+r+N-2) \end{bmatrix}$$

$$\mathbf{Y}_\mathbf{f} = \begin{bmatrix} \mathbf{y}(k+r) & \mathbf{y}(k+r+1) & \cdots & \mathbf{y}(k+r+N-1) \\ \mathbf{y}(k+r+1) & \mathbf{y}(k+r+2) & \cdots & \mathbf{y}(k+r+N) \\ \vdots & \vdots & \ddots & \vdots \\ \mathbf{y}(k+2r-1) & \mathbf{y}(k+2r) & \cdots & \mathbf{y}(k+2r+N-2) \end{bmatrix}$$

$$\cdots \text{(5-1, 2)}$$

$$\mathbf{X} = \begin{bmatrix} \mathbf{x}(k) & \mathbf{x}(k+1) & \cdots & \mathbf{x}(k+2r-1) \end{bmatrix} \tag{6}$$

In respective Eqs. (4) and (5), the scope is divided into two parts, the past and the future based on a certain time for the calculation reasons described later.

The matrix **Θ**, which is designated the expanded observability matrix, and **Ψ** are expressed as follows.

$$\mathbf{\Theta} = \begin{bmatrix} \mathbf{C} \\ \vdots \\ \mathbf{C}\mathbf{A}^{k-1} \\ \mathbf{C}\mathbf{A}^{k} \end{bmatrix},\ \mathbf{\Psi} = \begin{bmatrix} \mathbf{D} & & & \mathbf{0} \\ \vdots & \ddots & & \\ \mathbf{C}\mathbf{A}^{k-2}\mathbf{B} & \cdots & \mathbf{D} & \\ \mathbf{C}\mathbf{A}^{k-1}\mathbf{B} & \cdots & \mathbf{C}\mathbf{B} & \mathbf{D} \end{bmatrix}$$

$$\cdots \text{(7-1, 2)}$$

Others shown in Eq. (3) are notes related to noise, but they are not directly used in subsequent calculations, so we will omit them here and proceed with discussions.

In the MOESP method, the expanded observability matrix **Θ** is estimated by using an Eq. (3), and the system matrix **A** and **C** are calculated. First, using the input and output data to execute the LQ decomposition shown in the following equation composed of the block Hankel matrix defined in Eqs. (4) and (5). The Eq. (8) is the LQ decomposition that can be placed in the Ordinary MOESP method is represented.

$$\begin{bmatrix} \mathbf{U}_f \\ \mathbf{Y}_f \end{bmatrix} = \begin{bmatrix} \mathbf{L}_{11} & \mathbf{0} \\ \mathbf{L}_{21} & \mathbf{L}_{22} \end{bmatrix} \begin{bmatrix} \mathbf{Q}_1^T \\ \mathbf{Q}_2^T \end{bmatrix}. \tag{8}$$

The block matrix $\mathbf{L}_{22}$ obtained by Eq. (8) is applied singular value decomposition as shown in Eq. (9). The block matrix $\mathbf{U}_1\mathbf{\Sigma}_1^{1/2}$ is an estimated value of the expanded observability matrix **Θ**.

$$\mathbf{L}_{22} = \begin{bmatrix} \mathbf{U}_1 & \mathbf{U}_2 \end{bmatrix} \begin{bmatrix} \mathbf{\Sigma}_1 & \mathbf{0} \\ \mathbf{0} & \mathbf{\Sigma}_2 \end{bmatrix} \begin{bmatrix} \mathbf{V}_1^{\mathrm{T}} \\ \mathbf{V}_2^{\mathrm{T}} \end{bmatrix} \approx \mathbf{U}_1\mathbf{\Sigma}_1\mathbf{V}_1^{\mathrm{T}} \tag{9}$$

The system matrix **A** is calculated from the expanded observability matrix **Θ**. The natural frequency f_j ($j = 1 \sim n$) and damping ratio h_j ($j = 1 \sim n$) are calculated using the eigenvalue λ_j of the system matrix **A**.

$$f_j = \frac{\left|\ln \lambda_j\right|}{2\pi\Delta t}, \quad h_j = -\frac{\ln\left|\lambda_j\right|}{\left|\ln \lambda_j\right|} \tag{10-1, 2}$$

2.2 SETTING CALCULATION CONDITION

In the Ordinary MOESP method, it is necessary to adjust the system number N and the number of lines r of the block Hankel matrix. In Previous research [2], we find the two indicators shown in the following equations can accurately determine the system number N and the number of lines r in each time section.

$${}_1e_i = \frac{\sqrt{\left(\sum_{i=1}^{n} {\sigma_i}^2\right)^{\frac{1}{2}}}}{\left(\sum_{i=1}^{rl} {\sigma_i}^2\right)^{\frac{1}{2}}} \times 100 \tag{11}$$

$${}_2e_i = \sqrt{\frac{\sum_{i=1}^{N_k} \left({}_rZ_i - {}_{ave}Z_i\right)^2}{N_k}} \tag{12}$$

Where N_k means the total number of time intervals when the input and output data are divided into multiple intervals on the time axis, and ${}_rZ_i$ is the frequency and damping ratio which identified in time interval i. ${}_{ave}Z_i$ represents the average value of all block rows of frequencies and/or damping ratio identified in time interval i.

As a result of the preliminary examination, it was determined that appropriate calculation results could be obtained for values exceeding 98% of the index ${}_1e_i$ in each time interval. In addition, since it is necessary to secure a

https://doi.org/10.52202/069179-0306

sufficient number of Hankel rows in order to ensure the accuracy of identification, the upper limit was set to the number of Hankel rows.

In accordance with the above-mentioned identification method, dynamic characteristics can be calculated by using earthquake observation. To investigate the time dependent changes in these characteristics, the observed time history is split into 4 s, and a half of this dividing time is processed for each computation.

3 SEISMIC PERFORMANCE OF WOODEN TEMPLE EVALUATED BY EARTHQUAKE OBSERVATION

3.1 SEISMIC OBSERBATION FOR REINFORCED WOODEN TEMPLE

The target building is a wooden one-story temple the roof is copper tiled, the height of the building is about 9.5 m, the plane is about 14 m × 19 m. The timber, that constructs the main frame, is almost entirely Japanese pine, and parts of the columns are composed of zelkova serrate. The primary structural frame is made with post and beam construction. The main aseismic elements of the vertical plane include traditional mud walls and hanging walls finished with ordinary plaster, and the building was seismically retrofitted in 2013 through 2014 by adding to Plywood. the outline is shown in the Fig. 2. As shown in the Fig. 2, accelerometers are installed at 7 locations in the temple for seismic observation. These are the same as the seismometer arrangement before reinforcement reported in the previous study [3].

Acceleration data from 2012 to 2019 can be obtained. All sensors were able to measure to a limit 1500 cm/s (resolution: 0.01 cm/s) at intervals of 0.01 s, and to record acceleration in three directions. Sensors 1 and 2 observed input motions; the other sensors, located on girders on the roof frame, observed the seismic responses of this target building.

As system identification, the assumed characteristics include that the orthogonal directions, which means the X- and Y-directions shown in Fig. 2, affect each other, therefore cannot be operated independently in each direction. In this paper, the following results are computed for a two input (the records of X- and Y- directions by Sensor-2) and ten output (the records of X- and Y-directions by Sensors 3~7) system. Sensor 1 is not used in this study because Sensor 2 can represent the feature of input motion by previous research [3].

3.2 THE EARTHQUSKE OBSERVATION

Many observational results were obtained during the period from 2012 to 2019, including the issue of trigger settings. In this study, observation records were selected on the condition that PGA in at least one of the two horizontal directions exceeded 10 gal. 44 seismic observation records satisfy these conditions, and the system identification results for these are shown below.

For reference, the observed waveforms in the X and Y directions on July 17, 2016, when the maximum PGA was recorded, are shown in Fig. 3, and the response spectrum obtained from them is shown in Fig. 4.

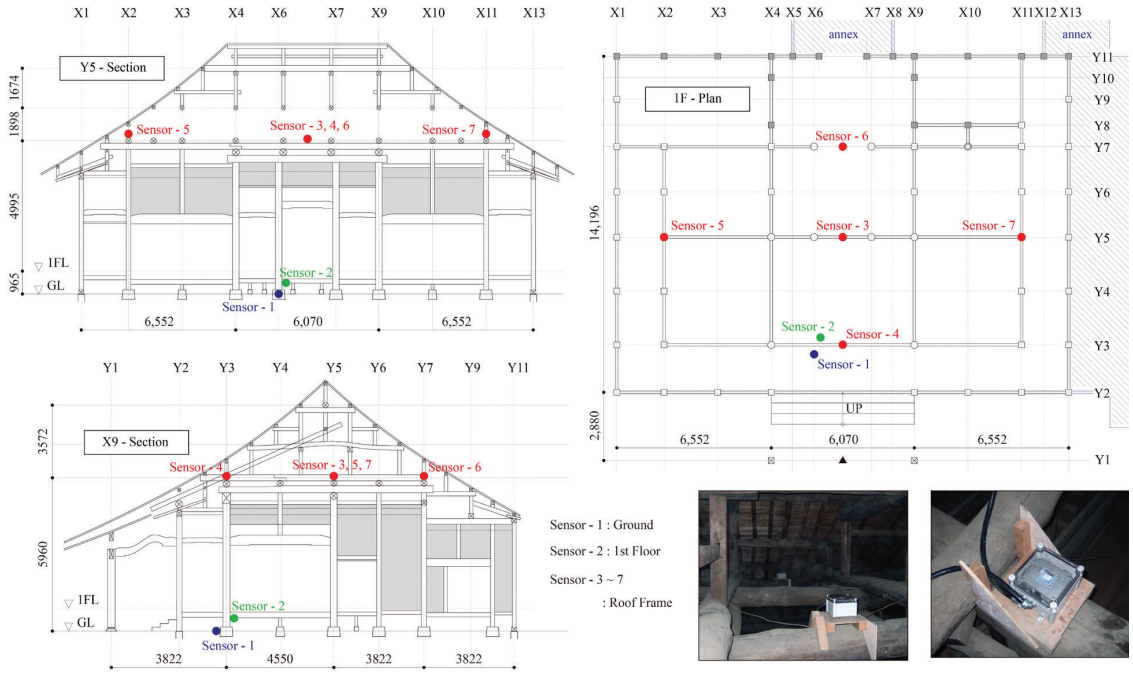

***Figure 2**: Outline of the measuring points on the earthquake observation* [3]

https://doi.org/10.52202/069179-0306

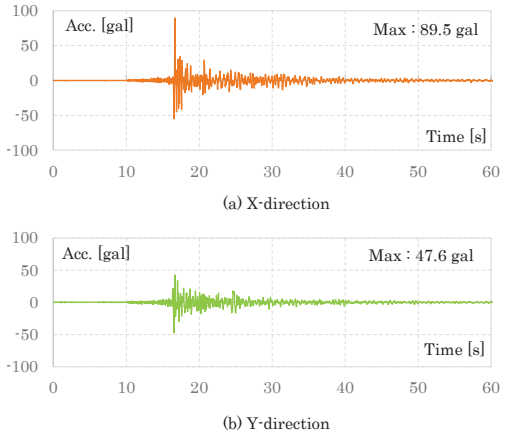

***Figure 3**: Acceleration time history (17th, July, 2016)*

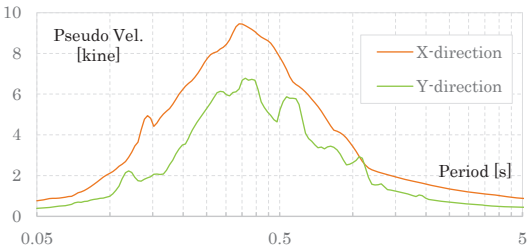

***Figure 4**: Pseudo velocity response spectrum (17th, July, 2016)*

As can be seen in Fig. 3, there is no standard definition of earthquake duration. In this paper, using the effective duration evaluated by the following equation [4] as a measure, we cut off the calculation target interval from each observation record. In addition, in order to remove high-frequency noise that can also be seen in the waveform of Fig. 3, processing was performed using 0.5 through10 Hz bandpass filter.

$$a(t) = \frac{\int_0^{t_0} \ddot{z}^2(t)\,dt}{\int_0^{t} \ddot{z}^2(t)\,dt}$$

Where $a(t)$ means the time history with no dimension of acceleration power, $\ddot{z}$ (t) denotes the acceleration of ground motion, t_0 denotes target time. When $a(t)$ is in the range of

$$0.01 \le a(t) \le 0.95\,,$$

the duration of earthquake is verified the efficiency in this research.

The Fourier spectrum shown in Fig. 4 indicates that the dominant frequency recorded in this earthquake is approximately 3 Hz. Most of the observation records investigated in this study are intraplate earthquakes, which, like this record, are dominated by relatively short periods of 1Hz or more. We add that the target temple also responds clearly to these seismic motions, since it also has a relatively short period.

3.3 UNDERSTANDING THE EFFECT OF NONLINEARLITY

As a result of system identification, Fig. 5 shows the change over time of the natural frequency and story drift for the earthquake that recorded the maximum ground acceleration in the observation record, which discusses Fig. 3 and 4. The story drift is calculated by integration of the acceleration data recorder by Sensor-2 and 3 on each direction.

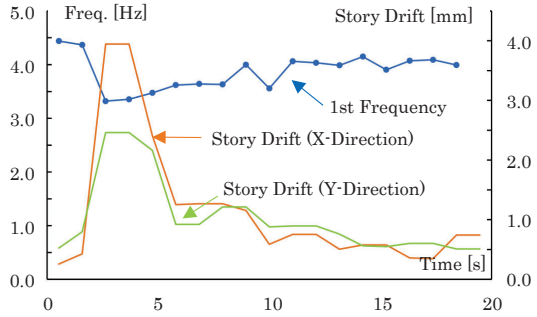

***Figure 5**: Changes in natural frequency and story drift over time estimated by the records on 17th, July, 2016*

Fig. 5 shows that the natural frequency is about 1 Hz as the story drift increases. This is considered to be the result of the nonlinearity of the strain-dependent of a timber structure. In addition, comparing the natural frequency before and after the earthquake, it is also suggested that a decrease of about 0.5 Hz has been observed, causing damage.

In order to confirm the change in vibration properties due to nonlinearity, comparing the vibration mode for each range of story drift corresponding to the identification results shown in Fig. 5. Fig. 6. shows a result comparing the vibration mode of each deformation range. The figure is created by standardizing the maximum value to 1.0 among the eigenvalue mode in each measurement position, and also taking into account the phase difference of each channels.

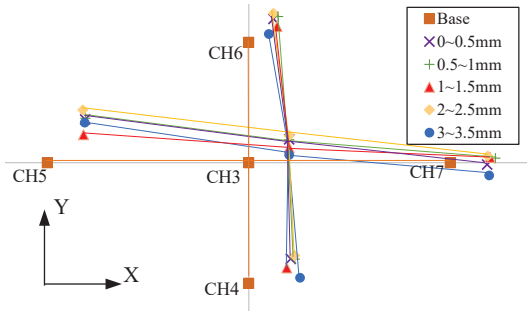

***Figure 6**: Comparison of vibration mode due to difference of story drift estimated by the records on 17th, July, 2016*

All vibration mode is not the same, but no significant difference is observed as shown in Fig. 6. From the above-mentioned results, it is presumed that the vibration properties itself do not change significantly even if the natural frequency due to nonlinearity is reduced.

https://doi.org/10.52202/069179-0306

3.4 INVESTIGATING THE TREND FOR LONG OBSERVSTION PERIOD

Following the discussion of short-term natural frequency changes in the same earthquake described above, only long-term changes are investigated. Fig. 7 shows the average values obtained from the identification results of each observation record, arranged in order by observation period. In this figure, the seasons are color-coded.

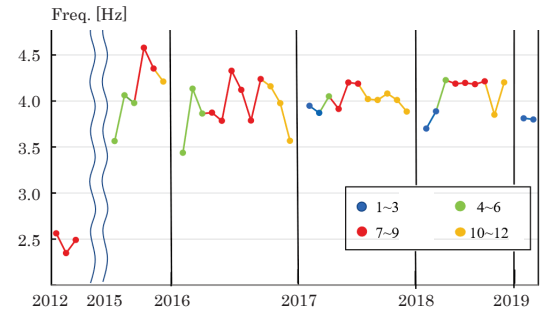

(a) Long-term change of the natural frequency

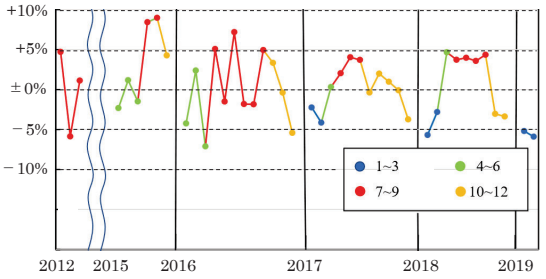

(b) the range of changing caused by seasons

***Figure 7**: Changes in natural frequency for Long-period*

From Fig. 7 (a), it can be confirmed that the natural frequency is greatly improved by the seismic reinforcement, and also can be seen that there is a certain amount of periodic variation in each season. In order to clarify the range of seasonal fluctuations, the Fig. 7 (b) shows the results standardized by the average value for before and after seismic retrofit respectively. From this result, it can be seen that the seasonal variation is about 10 % for the natural frequency, and about 20 % for the stiffness assuming that the mass is the same.

4 ANALYSIS OF LONG-TERM STRUCTURAL PERFORMANCE

4.1 CHANGES IN VIBRATION CHARACTERISTICS DUE TO THE SURROUNDING ENVIRONMENT

We investigate the factors that affect the change in the natural frequency of traditional wooden buildings. Fig. 8 shows a comparison between the outside temperature at the location of the target temple, where is Kasukabe-city, Saitama prefecture (near Tokyo), and the natural frequency for each seismic response of story drift. The temperature is the average of the day published by the Japan Meteorological Agency [5]. In the same figure, symbols are displayed separately for each story drift, and the reasons that the multiple results are plotted on the same horizontal axis, is given multiple identification results as the same event as shown in Fig. 5. In addition, the horizontal axis does not show the real time, but the events that occurred in the year are arranged in order of occurrence.

From Fig. 8, it can be seen that the natural frequency decreases as story drift increases, as in the previous result. First, in order to understand the overall trend, focusing on the results of deformation of 0.5 mm or less, which is the most identified result as the equivalent deformation range,

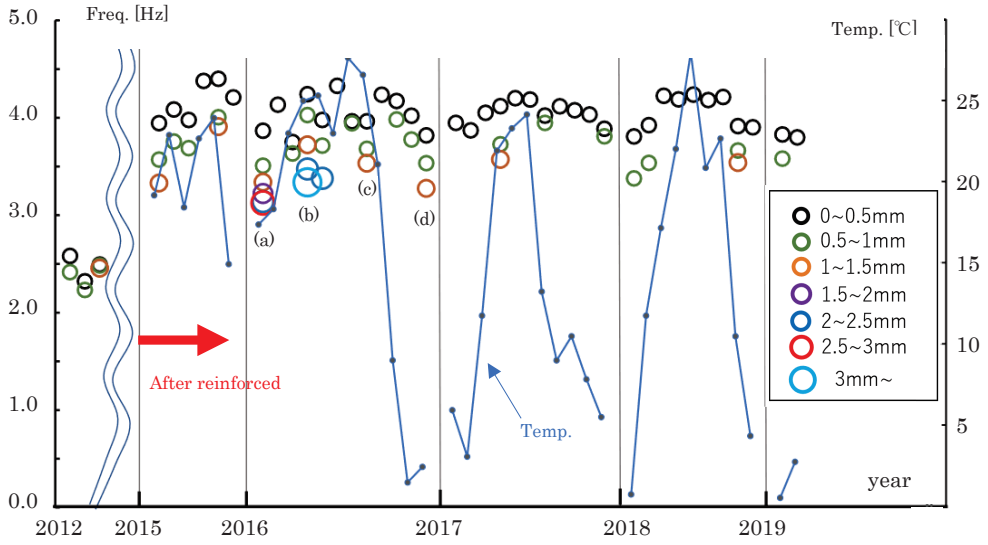

***Figure 8**: Changes in natural frequency for each story drift due to seasonal changes*

https://doi.org/10.52202/069179-0306

it can be seen that the natural frequency has been gradually decreasing since 2015 after the seismic reinforcement. There are two possible reasons. One is the accumulation of damage caused by earthquakes, and the other is the viscoelastic property of wood. The former was also confirmed in the results of Fig. 5, suggesting that there are factors that accumulate in addition to changes in the natural frequency due to nonlinearity. The latter does not even have method to assess its impact. Although there is a possibility that the result was obtained because it was a traditional wooden building where the properties of wood are likely to appear, it is considered to be a problem that can occur in all timber structures.

Next, focusing on the correspondence between the temperature and the natural frequency of the surrounding environment, it can be seen that the natural frequency clearly increases as the temperature increases, and conversely, the natural frequency decreases as the temperature decreases. It is understood the reason that the wood swelled due to the increase in the amount of moisture in the air accompanying the temperature rise, and conversely, the wood contracted due to drying accompanying the temperature drop. The effect is relatively large, because it can be evaluated that the change corresponding to the decrease in the natural frequency for about five years, which discussed above, is repeated in one year.

Finally, in order to confirm the changes in the vibration properties accompanying these changes in the natural frequency, Fig. 9 shows the comparison results of the eigenmodes for the same seasons during three years from 2016, and Fig. 10 shows the comparison results of the eigenmodes identified for the events (a) to (d) appended to Fig. 8, which means the changes occurring over the course of one year. From the results shown in both figures, it is verified that even if some factors change the natural frequency, there is no significant effect on the vibration characteristics. This view is based on various pre-conditions such as the appropriateness of the arrangement of seismic elements, but it is an important property confirmed in this study.

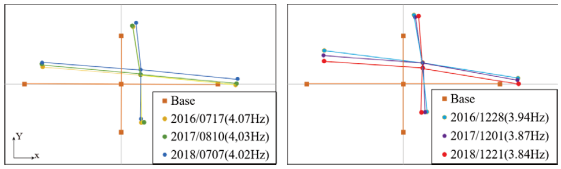

(a) Hot seasons *(b) Cold seasons*

***Figure 9**: Comparison of vibration mode in hot and cold seasons*

5 CONCLUSIONS

In this paper, the subspace method is applied to the observation records of traditional wooden buildings, and the transition of natural frequency over time is verified along with the changes in the environment. The findings are summarized as follows.

- The natural frequency changed as the temperature up and down, suggesting the effect of swell and shrink of the wood composed the target temple.
- It was confirmed that even if the natural frequency changes depending on the surrounding environment, there is no significant difference in the vibration characteristics.
- In the small deformation range about less 3 mm, the variation in the natural frequency may have the same effect as the nonlinearity due to the large and small response.

ACKNOWLEDGEMENT

We would like to our sincere gratitude toward the chief priest of Jyou - syun - in, Seihou Ishida and sub-chief, Ri-gyou Ishida for their help during this earthquake observation; and former assist. prof. Takenori Hida, Tokyo Univ. of science, for advice about system identification. A part of this study was carried out under support by Junichiro Hara and Naoki Tomiyama, former graduate students, to compute identification results and to organize the data.

REFERENCES

[1] Verhaegen, M. and Verdult, V. : Filtering and System Identification A Least Square Approach, Cambridge University Press, 2012. 7

[2] Hara, J. and Sato, T. : Applicability of subspace method to MIMO systems based on identification error - Accuracy verification of three calculation methods for timber structures -, Journal of Structural and Construction Engineering (Transaction of AIJ), 2023 (in preparation).

[3] Sato, T., Nagano, M. and Mochizuki, E : Seismic Performance of A Wooden Temple Inferred from Earthquake Observation and Seismic Diagnosis, WCTE 2014, Quebec, 2014. 8

[4] Akiyama, H. and Kitamura, H. : Relationship between energy spectra and velocity response spectra, Journal of Structural and Construction Engineering (Transaction of AIJ), No. 608, pp.37-43, 2006. 10 (in Japanese).

[5] Japan Meteorological Agency (/www.jma.go.jp)

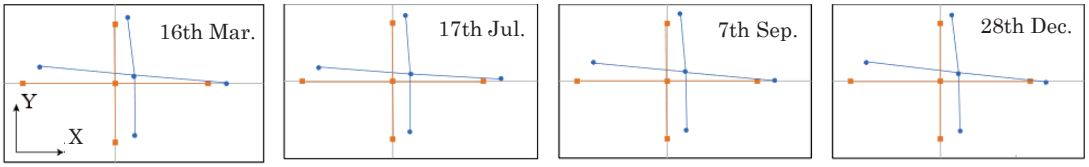

(a) Record – a *(b) Record – b* *(c) Record – c* *(d) Record – d*

***Figure 10**: Comparison of vibration mode changing by seasons*

https://doi.org/10.52202/069179-0306